De-localizing brittle fracture

Oguz Umut Salman, L Truskinovsky

De-localizing brittle fracture

Preprint · November 2020

CITATIONS
0

READS
52

2 authors, including:

Oguz Umut Salman
French National Centre for Scientific Research
31 PUBLICATIONS **297** CITATIONS

SEE PROFILE

De-localizing brittle fracture

O.U. Salman[a], L. Truskinovsky[b]

[a]LSPM, CNRS - UPR 3407, Université Sorbonne Paris Nord, 93430 Villetaneuse, France
[b]PMMH, CNRS - UMR 7636 PSL-ESPCI, 75005 Paris, France

ARTICLE INFO

Keywords:
Metamaterials, quasi-brittleness, ductility, micro-cracking, damage, fracture, high gradients, phase-field.

ABSTRACT

Localization of damage in conventional brittle materials is the source of a host of undesirable effects. In this paper, we show how artificially engineered metamaterials with all brittle constituents can be designed to ensure that every breakable sub-element fails independently. The crucial role in the proposed design is played by high contrast composite sub-structures with zero-stiffness, furnishing nonlocal stress redistribution. The de-localized cracking of the resulting nominally brittle systems can be linked to the fact that their continuum description is dominated by gradient rather than classical elasticity. By engineering a crossover from brittle to effectively ductile (quasi-brittle) behavior, we elucidate the structural aspects distinguishing macro-cracking-dominated fracture from micro-cracking-dominated damage.

1. Introduction

Brittle materials fail with the development of a system-size crack which originates from a microscopic flaw and advances by focusing singular stresses near the tip [1, 2]. Such extreme stress localization can be traced to the non-convexity of the inter-atomic potential [3, 4] leading to softening of elastic response with eventual loss of ellipticity of equilibrium equations [5, 6]. In applications, brittleness is often a source of undesirable effects from low toughness to the catastrophic character of dynamics [7, 8].

Many ingenious strategies for tempering brittleness and creating effective ductility have been proposed in the literature, including toughening by micro-cracking [9, 10], rigidity mitigation [11], engaging phase transformations [12, 13] and utilizing multi-level failure mechanisms [14, 15]. The idea is to avoid the unstable crack propagation [16] by creating obstacles and dissipation centers [17, 18, 19] that can trap the system in a meta-stable configurations [20, 21]. It was shown that such crack-channeling mechanisms can be tailored to achieve high energy absorption and that the resulting nominally brittle artificial materials can rival their natural ductile analogs [22, 23, 24].

In this paper, we propose a fundamentally different approach to fracture de-localization. The idea is to balance progressive softening of the material by strengthening of the nonlocal interactions ensuring stress redistribution and preventing strain localization. The task of transmitting nonlocal interactions is assigned to a distributed sub-structure of effective backbones whose elasticity is bending dominated.

As a proof of principle, we develop here a prototypical model of a mechanical system with nominally brittle constituents at the micro-scale. It is intended to show a crossover from the conventional elastic behavior at small tensile loading (and no damage) to the bending dominated elastic response at considerable tensile loading (and appreciable damage). We show that such transition ensures that instead of softening induced failure localization, the emerging nonlocal elasticity redistributes the stress globally so that every single brittle sub-element breaks independently. The proposed design, relying on the stabilization of floppy modes by bending, has a bio-mimetic nature as it structurally imitates some known biological prototypes [25, 26]. The proposed composite structure with variable-connectivity can be built already using conventional techniques of additive manufacturing.[27].

Our approach is deliberately minimalistic as we deal only with the most simple one-dimensional local (softening) and nonlocal (bending dominated) elastic sub-structures. The local sub-structure is represented by a chain of springs with Lennard-Jones type nonconvex potential. The nonlocal sub-structure, is a zero-stiffness pantograph built of inextensible but flexible beams connected through pivots [28, 29]. The two sub-structures are coupled in such a way that in the initial state, where all breakable springs are intact, the whole system is over-constrained [30, 31]. As the structure is stretched, the geometrical constraints force the breakable elements to fail, and the composite mechanical system progressively transforms into an under-constrained one with dominating bending (gradient) elasticity. While we use only the simplest nonlocal sub-structure in our analysis, other intentionally floppy structural designs could be

ORCID(s): 0000-0003-0696-521X (O.U. Salman)

used as well [32]. A general analysis of such systems can be found in the theory of high contrast elastic composites [33, 34]. in whose homogenized continuum representation, the higher-order elasticity appear already at the leading order bringing into the theory an internal length scale [35, 36, 37].

We recall that, in the absence of a floppy reinforcing sub-structure, a chain of breakable springs loaded in tension fails abruptly with a formation of a single macro-crack [38]. Here we show that the same system with the reinforcement breaks gradually and exhibits distributed micro-cracking. The whole process can be interpreted as damage spreading or even viewed as a propagating phase transition front separating affine and non-affine deformation states. Most remarkably, we show that, due to the presence of nonlocal reinforcement, the affine deformation is recovered at a sufficiently large level of stretching with strain uniformity now being enforced exclusively by bending elasticity. Such re-entrant homogeneity of deformation distinguishes the nonlocal brittle structure from the conventional local brittle solid, which cannot 'heal' the developed deformational non-affinity in monotone tension.

In a continuum framework, the proposed composite structure can be modeled as a softening elastic bar with a strain gradient term in the energy representing bending elasticity. The resulting continuum model takes the classical Ginzburg-Landau (GL) form with macroscopic strain playing the role of order parameter [39, 40] and the usual double-well energy replaced by a Lennard-Jones type potential. A model of this type was considered in [41] under the assumption that 'bending stiffness' diminishes with deformation, which cancels the re-entry effect. Another related model is a strain gradient regularization of damage mechanics [42] with the unrealistic assumption that the nonlocal stiffness is independent of damage [43].

A conceptual link can also be built with models developed to describe ductile fracture in plastic solids where the authors use the deformation theory of plasticity and complement the effective local energy by an additive weakly nonlocal term describing strain gradient hardening [44, 45].

We show that the appropriately calibrated GL continuum model reproduces all the essential features of our prototypical discrete structure, including the propagating damage fronts and the re-entrant behavior. We also consider a version of the GL model with a constraining linear elastic environment, which is particularly relevant for biological applications [46]. In this setting, the effectively ferromagnetic interactions implied by bending elasticity compete with effectively anti-ferromagnetic interactions brought by the elastic background. The resulting mechanically frustrated system is shown to generate patterns with alternating affine and non-affine behavior.

If the nonlocal reinforcement is removed, the remaining local sub-structure represents a conventional brittle material that can be simulated using the gradient damage model [47, 48, 49, 50] or any other version of the phase-field model of fracture [51, 52, 53, 54]. We show that in this case, neither the distributed damage nor the re-entrant behavior occurs. Even when the elastic environment is present, the broad non-affine zones are absent in this setting, being replaced by the pattern of highly localized macro-cracks.

The rest of the paper is organized as follows. In Section 2, we introduce the discrete model of the pantograph-reinforced breakable chain and show that fracture in this system is de-localized. In Section 3, we build a continuum version of the same system and show that it is fully faithful to its discrete prototype. In Section 4, we study the case when the continuum model is constrained by an elastic environment and obtain regular patterns of alternating affine and non-affine behavior. In Section 5, we compare the behavior of the reinforced chain with the behavior of the corresponding brittle system represented by a phase-field model. In the final Section 6, we present our conclusions.

2. Meta-material design

To motivate further developments, consider a conventional mass-spring chain constrained to remain on a straight line, see Fig. 1. The goal of this basic pre-model is to mimic the mechanical behavior of a softening nonlinear elastic material. To this end, we assume that the springs are 'breakable' and that their mechanical response is described by a non-convex elastic potential of Lennard-Jones type.

Figure 1: A chain of particles connected in series by breakable springs and loaded in tension.

Define the horizontal displacement u_i of the mass point with index i. Then the energy of the chain can be then

written in the form

$$E_S = a \sum_{i=0}^{N-1} f\left(\frac{u_{i+1} - u_i}{a}\right) \tag{1}$$

where $a = 1/N$ is dimensionless reference length. For our numerical illustrations, concerned exclusively with tension, it will be sufficient to use an analytically convenient expression for the elastic potential $f(x) = x^2/(2+x^2)$ where $x \geq 0$, see Fig. 2.

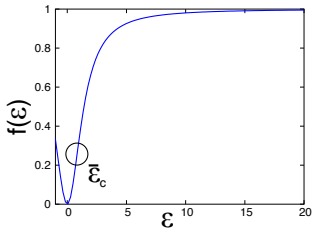

Figure 2: The Lennard-Jones-type elastic potential of a 'breakable' spring $f(x)$ which we use in our numerical experiments simulating tensile loading. Here $\bar{\varepsilon}_c$ is the turning point where the affine response of the mass spring chain with nearest interactions shown in Fig. 1 becomes unstable.

Suppose next that the chain, defined by the energy (1), is stretched quasi-statically in a hard device so that $u_0 = -\bar{\epsilon}/2$ and $u_{N-1} = \bar{\epsilon}/2$. Here $\bar{\epsilon} > 0$ is the average strain which will play the role of loading parameter. To find the response we need to solve the equilibrium equations $\partial E_S/\partial u_i = 0$ with $1 < i < N-2$ for each value of $\bar{\epsilon}$. Stable equilibria can be chosen using energy minimizing algorithms mimicking overdamped viscous dynamics. In this framework, quasi-static loading protocol, implying zero effective viscosity limit, maintains the system in a local minimum of (1) till it ceases to exist and then during isolated switching events performs the selection of new equilibrium branches [55]. Later in the paper we also discuss the global minimum path which implies at each value of the loading parameter the absolute energy minimization. This branch selection strategy, which is not realistic in the standard fracture setting, can be viewed as a parametric description of a quasi-static thermal equilibrium in the zero temperature limit.

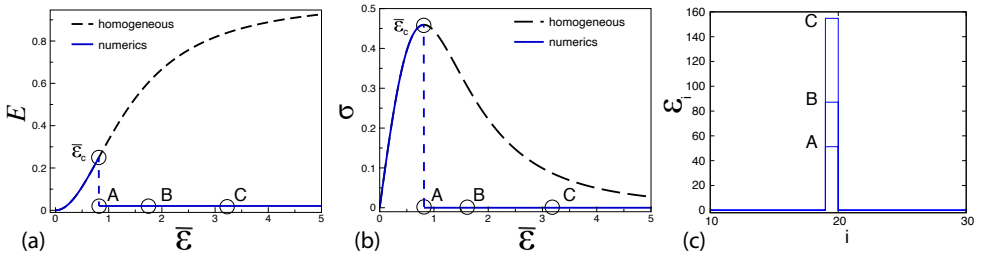

Figure 3: Mechanical response of a simple chain with breakable springs, see (1) , subjected to quasi-static tensile loading in a hard device: (a) the equilibrium elastic energy $E_S(\bar{\epsilon})$ and, (b) the equilibrium stress $\sigma(\bar{\epsilon}) = dE_s/d\bar{\epsilon}$, (c) the equilibrium strain profiles $\epsilon_i(\bar{\epsilon})$. Here $N = 50$.

To illustrate the classical brittle fracture with ultimate (lattice scale) strain localization, we simulated a tensile stretching of the chain with energy (1) and $N = 50$, see Fig. 3. Our incremental energy minimization approach involves L-BFGS iterations [56] (imitating gradient flow) until the gradient norm, which we use in our convergence criterion, is smaller than 10^{-6}. We then use the obtained pre-solution as an initial condition in Newton's method [57], which then furnishes the final solution. After the loading parameter is increased, the same protocol is repeated.

In Fig. 3 we show separately the equilibrium macroscopic energy, $E_s(\bar{\epsilon})$, the equilibrium macroscopic stress $\sigma(\bar{\epsilon}) = dE_s/d\bar{\epsilon}$ and the equilibrium distribution of the microscopic strain $\epsilon_i = (u_{i+1} - u_i)/a$ at the typical values of the loading parameter $\bar{\epsilon}$. As it is well known, the configuration in this case remains homogeneous (affine) till the loading parameter reaches the value $\bar{\epsilon}_c$ where $\partial^2 f/\partial\varepsilon^2 = 0$, see Fig. 2. At this value of loading, the affine elastic branch becomes unstable, and the stress drops to zero, see Fig. 3(b), as the strain abruptly localizes at the scale of the lattice, see Fig. 3(c). The

location of the newly formed localized crack is accidental (controlled by an initial imperfection), and the only result of the subsequent loading is the increase of its opening, see Fig. 3(c). Note that the dissipation during such a purely brittle failure process, where essentially only one spring breaks, is considerably smaller than in the case of ductile damage propagation where each spring can be expected to break individually.

To de-localize brittle fracture illustrated in Fig. 3, we now reinforce the series connection of breakable springs by a *sub-structure* shown in Fig. 4. The role of the additional pantograph frame made of inextensible but bendable beams connected by ideal pivots is to ensure that stress gets uniformly redistributed. While this sub-structure has zero longitudinal macro-scopic stiffness in the sense that it does not resist affine deformations, the non-affine longitudinal deformations remain energetically penalized due to the bending of individual beams.

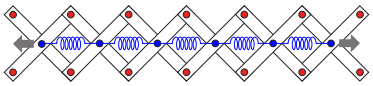

Figure 4: Floppy beam (pantographic) structure reinforcing a chain of breakable springs loaded in tension.

Suppose that such reinforced chain is again constrained to remain on a straight line. We can then write the (bending) energy of the beams inn the form

$$E_B = a \sum_{i=1}^{N-1} \frac{\lambda_1^2}{2} \left(\frac{u_{i+1} + u_{i-1} - 2u_i}{a^2} \right)^2, \tag{2}$$

where λ_1 is a dimensionless length proportional to a with the coefficient depending on the bending stiffness of the beams [58]. The total energy of the composite system is then

$$E = E_S + E_B. \tag{3}$$

We again load the system in a hard device with $\bar{\epsilon}$ being the loading parameter. No other constraints are imposed, making the ends of the reinforced structure effectively moment free [59].

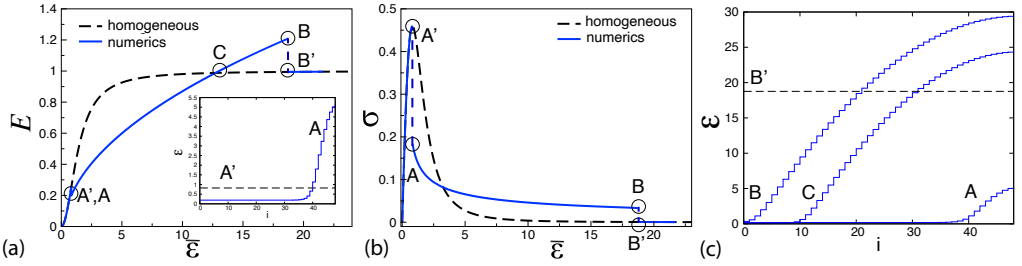

Figure 5: Quasi-static response of the composite system with $a = \lambda_1 = 0.02$: (a) the equilibrium elastic energy $E(\bar{\epsilon})$; (b) the equilibrium stress strain profiles $\sigma(\bar{\epsilon})$; (c) typical strain profiles. Under monotone quasistatic loading the homogeneous (affine) state A' transforms into an inhomogeneous (non-affine) state A. This transition can be interpreted as the nucleation of distributed damage at the boundary of the sample. The affine state is recovered when the inhomogeneous state B, describing a developed damage zone, transforms into the homogeneous state B'. This re-homogenization transformation would have happened at C if the system followed the global minimum path. Here $N = 50$.

The mechanical response of the reinforced chain is summarized in Fig. 5. As in the case of a simple chain, the energy minimizer is affine at sufficiently small values of the loading parameter. However, at a critical value of the load (point A'), we do not see the formation of an isolated localized crack. Instead the failure process starts with the formation of a diffuse nucleus representing partially damaged material at one of the boundaries of the sample (transition A'→A). As the loading continues, a diffuse zone of damage spreads through the structure. This process of successive micro-cracking is accompanied by a progressive decline of stress. The "de-localized" failure advances from A to B as more and more springs get broken, see Fig. 5(c). At another critical value of the loading parameter marked by B,

the damage abruptly spreads through the remaining, still-intact part of the sample and the deformation becomes again affine (transition B →B'). The newly acquired homogeneous response remains energy minimizing at larger strains.

If the simplest model of a breakable chain produces conventional localized fracture with an abrupt drop of stress and low dissipated energy, the model of a nonlocally reinforced chain shows an unusual de-localized fracture with a gradual decrease of stress and higher energy dissipation (compare the areas under the response curves in Fig. 3(b) and Fig. 5(b)). In other words, instead of breaking in two parts, as it is anticipated from a brittle system, the reinforced chain with breakable springs *fragments* uniformly into N equal parts.

3. Continuum model

To build the simplest (quasi) continuum approximation for the discrete model shown in Fig. 4 we need to consider a limit of small a and construct the lowest order asymptotically equivalent continuum energy functional still carrying a micro-scopic length scale a [60]. A straightforward expansion gives [61]

$$E = \int_0^1 \left(f(\varepsilon) + \frac{\lambda_1^2}{2}\varepsilon'^2 \right) dx, \tag{4}$$

where $u(x)$ is the continuum longitudinal displacement field and $\varepsilon = u'$ is the corresponding uniaxial strain. The energy density (4) maintains the additive structure of its discrete analog (3) with the first term representing the breakable springs and the second term describing the energy of bending. In our numerical illustrations we continue to use a particular function $f(\varepsilon) = \varepsilon^2/(2+\varepsilon^2)$ and the parameter λ_1 will again represent the dimensionless atomic length scale. To model the system loaded in a hard device we again set $u(0) = -\bar{\varepsilon}/2$, $u(1) = \bar{\varepsilon}/2$ where $\bar{\varepsilon} > 0$ is the imposed strain. Given that the boundaries of the bar are moment free we assume that $u''(0) = u''(1) = 0$. Under these assumptions the homogeneous (affine) configuration $u^0(x) = (\bar{\varepsilon}/2)(2x-1)$ is an equilibrium state at all $\bar{\varepsilon}$ which, however, is expected to become unstable due to strain induced softening of the energy f.

To investigate the stability limits of the homogeneous state we write a linear equation for the displacement perturbation $s(x)$ in the form

$$-\lambda_1^2 s'''' + \frac{\partial^2 f}{\partial \varepsilon^2}(\bar{\varepsilon}) s'' = 0 \tag{5}$$

The corresponding boundary conditions are: $s(0) = s(1) = s''(0) = s''(1) = 0$. The system becomes linearly unstable when

$$\frac{\partial^2 f}{\partial \varepsilon^2}(\bar{\varepsilon}) = -\lambda_1^2 (n\pi)^2, \tag{6}$$

with unstable mode $s(x) \sim \sin(n\pi x)$. The solutions of (6) for the chosen potential $f(\varepsilon)$ and different values of λ_1 are illustrated in Fig. 6(a).

If λ_1 is sufficiently small, the homogeneous (affine) configuration is stable in the two domains: for sufficiently small loadings $\bar{\varepsilon} \le \bar{\varepsilon}_c^*$ and for sufficiently large loadings $\bar{\varepsilon} \ge \bar{\varepsilon}_c^{**}$, see Fig. 6(b), with the same critical mode number $n_c = 1$ for both instabilities, see Fig. 6(c). This result suggests the existence in the interesting range of small λ_1 of a re-entrant, isola type bifurcation [62]. When dimensionless parameter λ_1 is large (large bending modulus or small system size), the affine state is stable for all values of the loading parameter $\bar{\varepsilon}$ which means that the failure takes place gradually and uniformly throughout the whole system.

The energy minimizing inhomogeneous (non-affine) configurations can be found by solving the nonlinear equilibrium equation

$$-\lambda_1^2 u'''' + \frac{\partial^2 f}{\partial \varepsilon^2}(u') u'' = 0 \tag{7}$$

with the boundary conditions on $u(x)$ formulated above. The whole set of solutions can be obtained in quadratures and analyzed in full detail. In particular, one can show that at $\bar{\varepsilon}_c^*$ the non-affine branch of equilibria with $n = 1$ bifurcates from the homogeneous state subcritically and then reconnects to it also subcritically at $\bar{\varepsilon}_c^{**}$; the same branch contains all nontrivial globally minimizing configurations. These general observations are illustrated in Fig. 7(a,b).

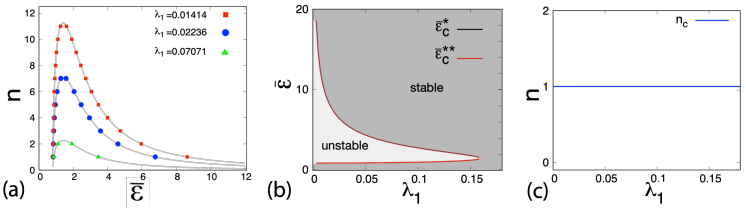

Figure 6: Linear stability of the homogeneous state in a model of nonlocally reinforced chain: (a) bifurcation points, (b) critical strains $\bar{\varepsilon}_c^*$ and $\bar{\varepsilon}_c^{**}$ (c) critical wave number n_c.

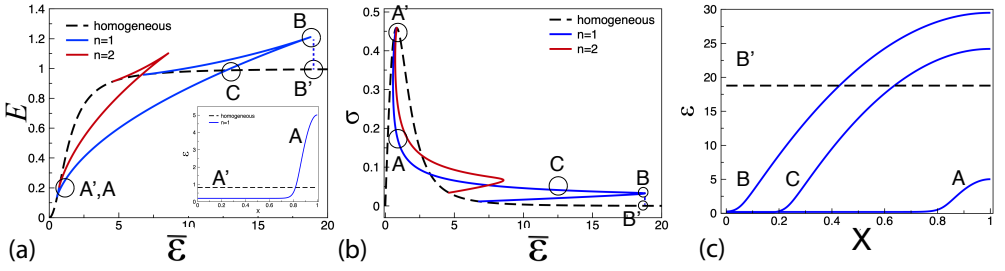

Figure 7: The response of the nonlocally reinforced chain : (a) equilibrium energy-strain relations showing the two lowest energy branches, (b) the corresponding stress-strain relations, (c) typical equilibrium strain profiles for the mode $n = 1$. The inset in (a) shows the nucleation of the diffuse damage zone near the boundary of the sample (transition A'→A). In point B the non-affine state transforms into the affine state (transition B→B'); along the global energy minimization path the same re-entry type transformation would take place in point C. The metastable equilibria corresponding to $n = 2$ are not reachable from the affine state under the assumption of overdamped dynamics. Here $\lambda_1 = 0.02$.

The structure of the energy minimizing strain fields can be seen in Fig. 7(c). Instead of sharp displacement discontinuities, characterizing brittle fracture, we observe diffuse damage zones. Instead of sharp transition zones characterizing conventional phase transitions, we observe broad transition layers separating the 'phases' of broken springs where $\partial^2 f/\partial\varepsilon^2 < 0$ and the dominating elasticity is of the bending (gradient) type, from the 'phases' of intact springs where $\partial^2 f/\partial\varepsilon^2 > 0$ and the dominating elasticity is still of the classical type.

The abrupt nucleation of the first domain of non-affinity takes place at $\bar{\varepsilon}_c^* > \bar{\varepsilon}_c$. In the linear regime the corresponding instability has a system size but then it partially localizes near the sample boundary in the nonlinear regime (transition A'→A). As the applied strain $\bar{\varepsilon}$ increases, the non-affine phase proliferates towards the other boundary of the sample while becoming progressively more inhomogeneous as successive springs continue to break. The affine state is recovered through the discontinuous event which marks the complete annihilation of the non-affine phase (transition B→B'), see Fig. 7(c).

The behavior of the continuum model is both qualitatively and quantitatively similar to what we have seen in the discrete model, see Fig. 5. In particular, in both models we observe the abrupt emergence and subsequent proliferation of the non-affinity zones which contain inhomogeneously ruptured springs as well as the abrupt recovery of the affine state as the rupture process saturates. The non-affine 'phase', stabilized by bending (gradient) elasticity, does not distinguish between individual micro-cracks and can be viewed at the macro-scale as the domain of developed damage. We can therefore conclude that the subject of damage mechanics is the delocalized micro-cracking emerging when the competing localized macro-cracking is inhibited due to nonlocal stress redistribution conducted by an under-constrained system of stress transmitting beams.

4. Elastic background

To show that the de-localized damage can also appear in the form of periodic spatial patterns, we now assume that our reinforced breakable chain is coupled to an elastic background. For analytical transparency we assume again that the parameter a is sufficiently small and adopt the quasi-continuum description encapsulated in (4).

Under the assumption that the elastic background is uniformly pre-stretched with the same strain $\bar{\varepsilon}$ as we apply on the boundaries of the chain, we can write the energy of the system in the form [63, 64]

$$E = \int_0^1 \left(f(\varepsilon) + \frac{\lambda_1^2}{2}\varepsilon'^2 + \frac{1}{2\lambda_2^2}(u - u^0(x))^2 \right) dx, \tag{8}$$

where $u^0(x) = (\bar{\varepsilon}/2)(2x-1)$ and λ_2 is a new dimensionless length scale characterizing the strength of the coupling between the breakable system and the linear elastic background. Note that in the expression (8) the elastic energy of the background proper is effectively subtracted.

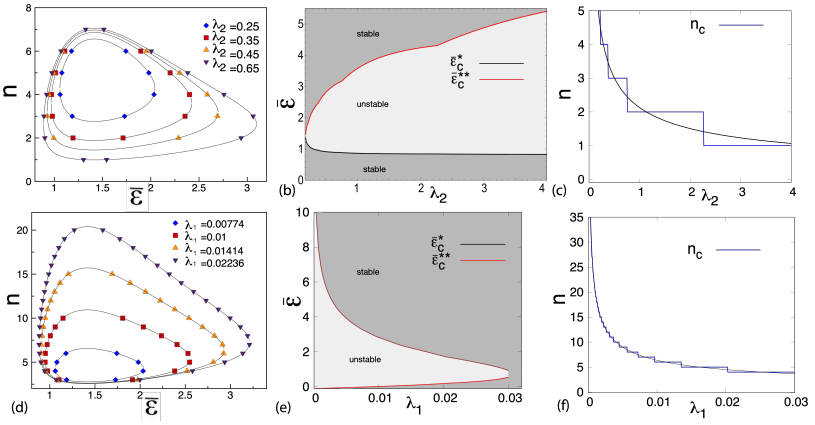

Figure 8: Linear stability limits for the reinforced chain coupled with an elastic background: (a,d) bifurcation points, (b,e) critical strains $(\bar{\varepsilon}_c^*, \bar{\varepsilon}_c^{**})$; (c,f) critical modes n_c. Parameters: in (a-c) $\lambda_1 = 0.02$. In (d-f) $\lambda_2 = 0.25$.

The instability/bifurcation condition for the homogeneous state takes the form

$$\lambda_1^2(n\pi)^4 + \frac{\partial^2 f}{\partial \varepsilon^2}(\bar{\varepsilon})(n\pi)^2 + \frac{1}{\lambda_2^2} = 0. \tag{9}$$

As in the problem without foundation, we obtain again that there are upper and lower critical strains $\bar{\varepsilon}_c^*$ and $\bar{\varepsilon}_c^{**}$ which again correspond to the same mode number n_c, however, now we can have $n_c \neq 1$, see Fig. 8. If we neglect the discreteness of the thresholds, we can write the approximating formulas $\partial^2 f/\partial\varepsilon^2(\bar{\varepsilon}_c) = -2(\lambda_1/\lambda_2)$ and $n_c = \pi^{-1}(\lambda_1\lambda_2)^{-1/2}$.

The dependence of solutions of (10) on parameters λ_1 and λ_2 is shown in Fig 8(a,d) while the bifurcation thresholds $\bar{\varepsilon}_c^*$ and $\bar{\varepsilon}_c^{**}$ are illustrated in Fig 8(b,e). One can see that the non-affinity can be suppressed if the bending stiffness λ_1 is sufficiently large or if λ_2 is small which means that the foundation-induced nonlocality is sufficiently strong. The wave number of the unstable mode tends to zero when either λ_1 or λ_2 disappears: the former case implies the disappearance of bending rigidity while the latter means the dominance of the elastic foundation, see Fig. 8(c,f).

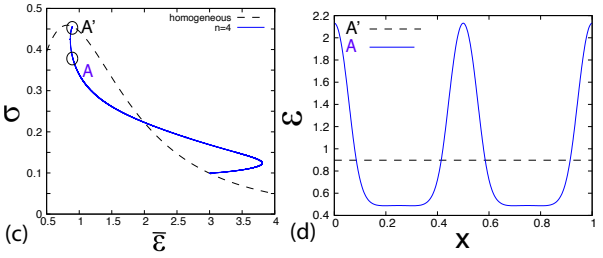

Figure 9: Pantograph reinforced chain coupled to an elastic foundation: (a) strain-stress relation along the first unstable branch showing the abrupt transition A'→A; (b) stable and unstable equilibrium profiles associated with the transition A'→A. Parameters: $\lambda_1 = 0.0167$, $\lambda_2 = 0.45$.

To reveal the post-bifurcational behavior we use the same boundary conditions as above, solve numerically the nonlinear equilibrium equation

$$-\lambda^2 u'''' + \frac{\partial^2 f}{\partial \varepsilon^2}(u')u'' - \frac{1}{\lambda_2^2}(u - u^0(x)) = 0. \tag{10}$$

and then trace the loading dependence of the response using the continuation algorithm [65]. The equation (10) describes the intricate interplay between the localization tendency due to nonconvexity of the energy $f(u')$, the coarsening effect of gradient elasticity which represents in this problem elastic interaction of the ferromagnetic-type, and the microstructure refinement favoring anti-ferromagnetic type interactions due to the elastic background [64]. The ensuing competition leads to the formation of finite scale periodic patterns which we illustrate in Fig. 9-11.

A detailed description of the first nucleation event at $\bar{\varepsilon} = \bar{\varepsilon}_c^*$ is shown in Fig. 9. The abrupt drop of stress at point A' indicates that the homogeneous state gets replaced by the islands of diffuse damage (transition A'→A). Since the linear instability at $\bar{\varepsilon}_c^*$ corresponds to $n = 4$, the emerging non-affine configuration is characterized by three symmetrically placed damage zones: one inside the sample and two on the boundaries, see Fig. 9(b).

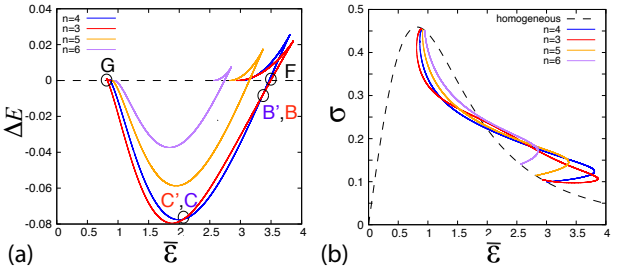

Figure 10: Quasi-static loading of a reinforced chain coupled to an elastic foundation: (a) the energy difference between the non-affine equilibrium configurations and the corresponding unstable affine configuration; (b) macroscopic strain-stress relations along different equilibrium branches; The transitions C'→C, B'→B and F→F' are the equilibrium branch switching events taking place along the global minimization path. Parameters: $\lambda_1 = 0.0167$, $\lambda_2 = 0.45$.

In Fig. 10(a) we show the strain dependence of the difference between the macroscopic energy of the affine configuration $f(\bar{\varepsilon})$ and the macroscopic energy of the bifurcated (non-affine) configuration $E(\bar{\varepsilon})$ from (8). The non-affine branches corresponding to different mode numbers n cross and all of them eventually reconnect with the affine branch. The macroscopic stress $\sigma(\bar{\varepsilon}) = dE/d\bar{\varepsilon}$ along the corresponding solutions of (10) is shown in Fig. 10(b).

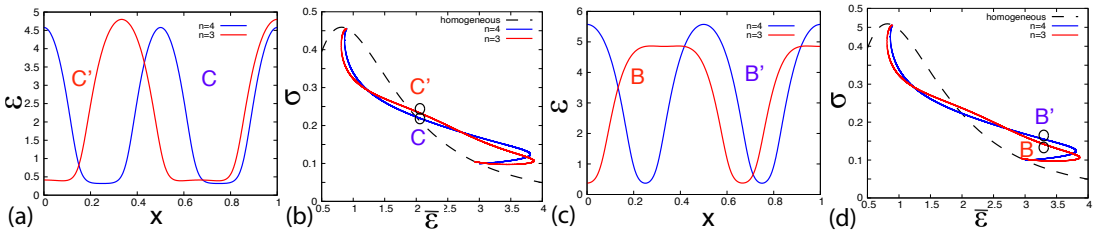

Figure 11: Branch switching events along the reversible global minimum path for the reinforced chain on elastic foundation foundation. Symmetry is lost during the C→C' transition and is recovered during the B'→B transition. Parameters: $\lambda_1 = 0.0167$, $\lambda_2 = 0.45$.

As the loading parameter $\bar{\varepsilon}$ increases, the domains of non-affinity grow till the strain threshold is reached when the remaining affine domains abruptly disappear and the homogeneous state gets restored. In Fig. 11, we illustrate some of the equilibrium branch-switching events taking place along the corresponding global minimization path. First, the non-symmetric configuration C' which is nucleated at point G, see Fig. 10(a), and corresponds to $n = 3$, undergoes a transformation C'→ C to the symmetric configuration corresponding to $n = 4$. As a result the second surface-bound damage zone appears, see Fig. 11(a,b). Then, we observe the reverse transition B'→B from the symmetric

configuration with $n = 4$ to the nonsymmetric configuration with $n = 3$. As the symmetry is lost one of the surface-bound diffuse damage zone disappears appears as it is illustrated in Fig. 11(c,d). Finally, the affine configuration is recovered when the symmetric state F with $n = 4$ abruptly transforms into the homogeneous state, see Fig. 10(a). We remark that the analysis of the global minimization path was presented above only for completeness of the picture. While the dissipation free nature of this path obviously fails to describe macroscopic material failure, it may still be relevant for the modeling of slowly loaded quasi-reversible cohesive biological systems.

To summarize, our analysis shows that, despite the brittle nature of the constituents, the material response of the reinforced chain is incompatible with the conventional scenario of highly localized cracking. Instead, our model predicts the emergence of de-localized damage zones which, in the presence of elastic background, advance from multiple sources. To show that in the case of conventional brittle cracking the elastic background cannot generate by itself similar pseudo-ductile response, we present in the next Section a detailed study of the chain with breakable elements coupled to the same elastic foundation but with the pantograph sub-structure removed.

5. Brittle fracture

For continuum representation of a simple chain with breakable elements, we use a phase-field computational approach [53, 49, 66]. In such theories, which also have the basic GL structure, the linear elastic stiffness degrades with damage described by a scalar variable [47]. The square of the gradient of this internal variable is usually chosen to control the energy cost of the ensuing non-affinity [67].

Suppose that the implied damage variable is $\alpha(x)$ with $\alpha = 0$ ($\alpha = 1$) corresponding to unbroken (fully broken) state. If the elastic environment is first neglected, we can then write the continuum energy of the system in the form

$$E = \int_0^1 \left(\frac{1}{2} g(\alpha)\varepsilon^2 + h(\alpha) + \frac{\lambda_1^2}{2}(\alpha')^2 \right) dx. \tag{11}$$

In (11), the first term, quadratic in strain, describes the linear elasticity of unbroken springs. The second term, independent of strain, is the energetic price of breaking. The third, regularizing term, penalizes the inhomogeneity of the phase-field $\alpha(x)$ and brings into the theory an internal length scale λ_1.

To find in this case the equilibrium mechanical response, we need to solve the system of nonlinear Euler-Lagrange equations

$$\begin{cases} (g(\alpha)u')' & = 0 \\ -\lambda_1^2\alpha'' + \frac{1}{2}\frac{\partial g}{\partial \alpha}(u')^2 + \frac{\partial h}{\partial \alpha} & = 0 \end{cases} \tag{12}$$

Our numerical experiments with the discrete chain shown in Fig. 1 will be matched if we assume that $g(\alpha) = (1-\alpha)^2$, $h(\alpha) = \alpha^2$ and choose the boundary conditions in the form $u(0) = -\bar{\varepsilon}/2$ and $u(1) = \bar{\varepsilon}/2$. Since the discrete theory does not operate with the phase-field variable $\alpha(x)$ directly, we choose at the ends the simplest natural boundary conditions $\alpha'(0) = \alpha'(1) = 0$. The homogeneous solution, representing in this case the principal branch of equilibria, is then described by the formulas: $u^o(x) = (\bar{\varepsilon}/2)(2x-1)$, $\alpha^o(x) = \bar{\varepsilon}^2/(2+\bar{\varepsilon}^2)$.

Denote by $s(x) \sim \sin(n\pi x)$ an admissible small perturbation of the displacement field $u^o(x)$ and by $\sigma(x) \sim \cos(n\pi x)$ the analogous perturbation of the phase-field $\alpha^o(x)$. Then the linear stability conditions for the principle branch of equilibria can be written as

$$(n\pi)^2 = -\frac{4\bar{\varepsilon}^2 \partial^2 f/\partial\varepsilon^2(\bar{\varepsilon})}{\lambda_1^2[(\partial f/\partial\varepsilon(\bar{\varepsilon}))\bar{\varepsilon} - \partial^2 f/\partial\varepsilon^2(\bar{\varepsilon})]}, \tag{13}$$

where we introduced the effective elastic energy $f(\varepsilon) = \varepsilon^2/(2+\varepsilon^2)$ which is obtained from the energy density $\frac{1}{2}(1-\alpha)^2\varepsilon^2 + \alpha^2$ by the adiabatic elimination of the phase-field variable (using the relation $\alpha \equiv \alpha^o$).

The λ_1 dependence of the solutions of (13) is illustrated in Fig. 12(a). We find that always $n_c = 1$, see Fig. 12(c). The λ_1 dependence of $\bar{\varepsilon}_c$ can be found from the equation

$$\bar{\varepsilon}_c(4\bar{\varepsilon}_c^2 - \lambda_1^2\pi^2)\frac{\partial^2 f/\partial\varepsilon^2(\bar{\varepsilon}_c)}{\partial f/\partial\varepsilon(\bar{\varepsilon}_c)} + \lambda_1^2\pi^2 = 0. \tag{14}$$

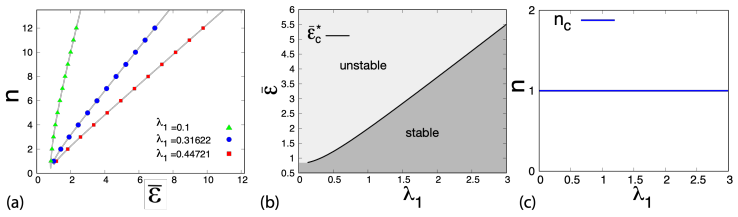

Figure 12: Phase-field model of brittle fracture: stability limits for the homogeneous state. Dependence on the regularization parameter λ_1 of: (a) bifurcation points; (b) critical strains $\bar{\varepsilon}_c$; (c) critical modes n_c.

which for our choice of the function $f(\varepsilon)$ reduces to $\lambda_1^2\pi^2 = 3\bar{\varepsilon}_c^2 - 2$, see Fig. 12(b). Note that in contrast to the case of the pantograph-reinforced chain shown Fig. 4, the affine configuration never re-stabilizes after the initial instability because the system remains singularly broken, see Fig. 12(b). Such response, however, is in full agreement with the behavior of the simple breakable chain shown in Fig. 1.

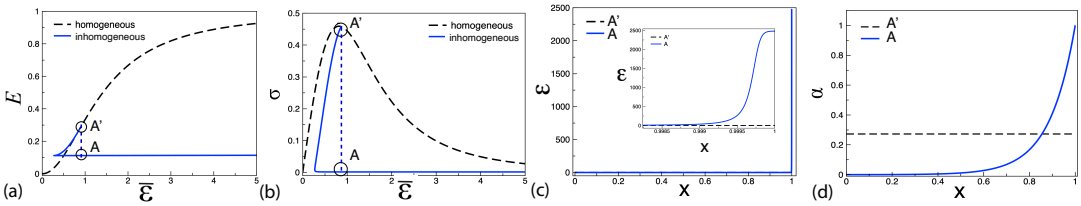

Figure 13: Overdamped phase-field model of brittle fracture is used to simulate the quasi-static stretching of an initially homogeneous brittle bar: (a) macroscopic energy-strain relation, crack nucleation takes the form of A'→A transition; (b) macroscopic stress-strain relation; (c,d) strain and damage profiles before and after the A'→A transition. Here $\lambda_1 = 0.158$

The representation of fracture localization in the phase-field model is illustrated in Fig. 13, where we show solutions of the nonlinear system (12) obtained by using Newton's method with arc-length continuation implemented as in [65].

The stretching response of this continuum system is basically the same as of the corresponding discrete model: a single crack forms abruptly (A'→A transition in Fig. 13(a,b)). The fact that the crack forms on one of the boundaries is due to a small bias due to the phase-field related boundary conditions. The subsequent loading leads to the increase of the amplitude of the localized strain. The only noteworthy difference between the behavior of the original discrete system and its continuum analog is a somewhat excessive smearing out of the crack caused by the phase-field regularization, see Fig. 13(c,d)

Given that our phase-field model reproduces adequately the mechanical response of a simple breakable chain we can consider next the behavior of the same chain coupled to an elastic background. The dimensionless energy in this case reads

$$E = \int_0^1 \left(\frac{1}{2} g(\alpha)(u')^2 + h(\alpha) + \lambda_1^2(\alpha')^2 + \frac{1}{\lambda_2^2}(u - u^0(x))^2 \right) dx, \tag{15}$$

and to find equilibrium configurations we need to solve the nonlinear system

$$\begin{cases} (g(\alpha)u')' - \frac{1}{\lambda_2^2}(u - u^0) & = 0 \\ -\lambda_1^2\alpha'' + \frac{1}{2}(u')^2\frac{\partial g}{\partial \alpha} + \frac{\partial h}{\partial \alpha} & = 0. \end{cases} \tag{16}$$

If the boundary conditions are kept the same as in the problem without the background, we obtain the same homogeneous solution and can define the same effective energy density $f(\varepsilon)$. In terms of this function, the linear stability

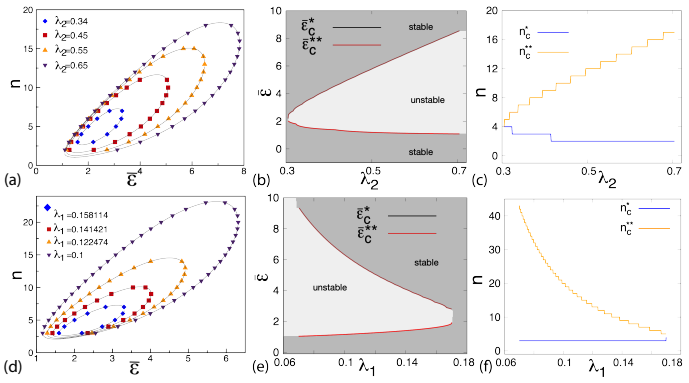

Figure 14: Phase-field modeling of a brittle bar coupled to an elastic environment: linear stability analysis; (a,d) bifurcation points; (b,e) critical strains $\bar{\varepsilon}_c^*$ and $\bar{\varepsilon}_c^{**}$; (c,f) instability mode numbers n_c^* and n_c^{**}. In (a-c) $\lambda_1 = 0.05$ and in (d-f) $\lambda_2 = 0.34$.

condition can be written in the form

$$\left[\frac{\lambda_1^2}{\lambda_2^2}\frac{f(\bar{\varepsilon}_c)}{\bar{\varepsilon}_c^2} + \frac{\partial^2 f}{\partial \varepsilon^2}(\bar{\varepsilon}_c)\right]^2 - \frac{\lambda_1^2}{\lambda_2^2}\frac{1}{\bar{\varepsilon}_c^2}\left[\frac{\partial f/\partial \varepsilon(\bar{\varepsilon}_c)}{\bar{\varepsilon}_c} - \frac{\partial^2 f}{\partial \varepsilon^2}(\bar{\varepsilon}_c)\right] = 0. \tag{17}$$

The critical mode number n_c can be found from the equation

$$(n_c\pi)^2 = -\left[(\frac{\lambda_1}{\lambda_2})^2\frac{f(\bar{\varepsilon}_c)}{\bar{\varepsilon}_c^2} + \frac{\partial^2 f}{\partial \varepsilon^2}(\bar{\varepsilon}_c)\right] \Big/ \left[\frac{\lambda_1^2}{2\bar{\varepsilon}_c^2}\left[\frac{\partial f/\partial \varepsilon(\bar{\varepsilon}_c)}{\bar{\varepsilon}_c} - \frac{\partial^2 f}{\partial \varepsilon^2}(\bar{\varepsilon}_c)\right]\right]. \tag{18}$$

In Fig. 14(a,d) we illustrate the parametric dependence of the solutions of (18). Due to the presence of elastic background the re-entry behavior of the affine configuration is recovered with the two critical strains $\bar{\varepsilon}_c^*$ and $\bar{\varepsilon}_c^{**}$ representing, respectively, the lower and upper limits of stability for the homogeneous state, see Fig. 14 (b,e). However, in contrast to the case of the pantograph-reinforced chain, the critical mode number $n_c(\bar{\varepsilon}_c^*)$ is now different from the critical mode number $n_c(\bar{\varepsilon}_c^{**})$, see Fig. 14 (c,f). This is because the re-stabilization (healing) of the affine state at large levels of stretching is of different physical origin in our two cases: the bending induced weak nonlocality in the case of the pantograph-reinforced chain and the elastic foundation induced strong nonlocality in the case of the elastically embedded chain.

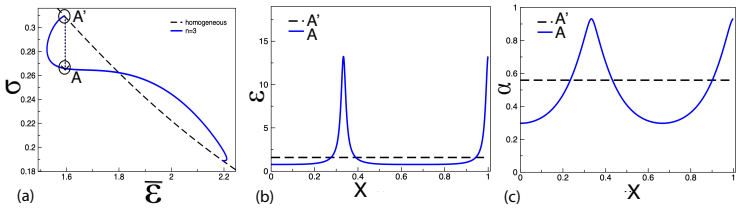

Figure 15: Brittle bar on elastic foundation: (a) Macroscopic stress strain response showing the discontinuous transition from affine to non-affine state at the critical strain $\bar{\varepsilon}_c^*$ (transition A'→A); (b,c) strain and phase-field profiles before and after the transition. Parameters: $\lambda_1 = 0.158$, $\lambda_2 = 0.34$.

The first branch switching event (transition A'→A) is shown in detail in Fig. 15. During this symmetry breaking transition we observe nucleation of two localized cracks, one inside the domain and one on the boundary, see Fig. 15(b,c). As a result of subcritical bifurcation, the principal branch (affine configuration) is replaced by the branch with $n = 3$, and this transition is accompanied by an abrupt stress drop, see Fig. 15(a).

After this initial collective nucleation event, the equilibrium configurations with larger number of localized cracks ($n = 3, ..., 7$) appear sequentially till finally at sufficiently large value of the loading parameter the strain localization

abruptly disappears and the damage becomes uniformly distributed. The corresponding solutions of the nonlinear system (16) are illustrated in Fig. 16 where we show the macroscopic energy for different equilibrium branches (rather the energy difference between the affine and the non affine configurations) and the corresponding stress-strain relations.

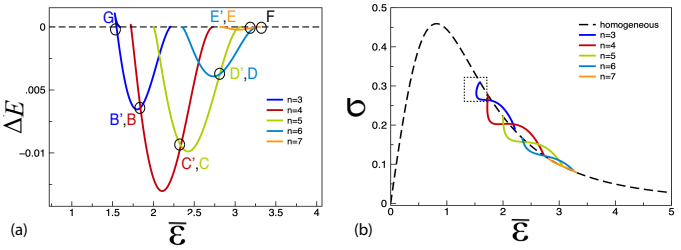

Figure 16: Brittle bar on elastic foundation: (a) the energy difference between the affine and various non-affine configurations ; (b) the corresponding macroscopic strain-stress response. Parameters: $\lambda_1 = 0.158$, $\lambda_2 = 0.34$.

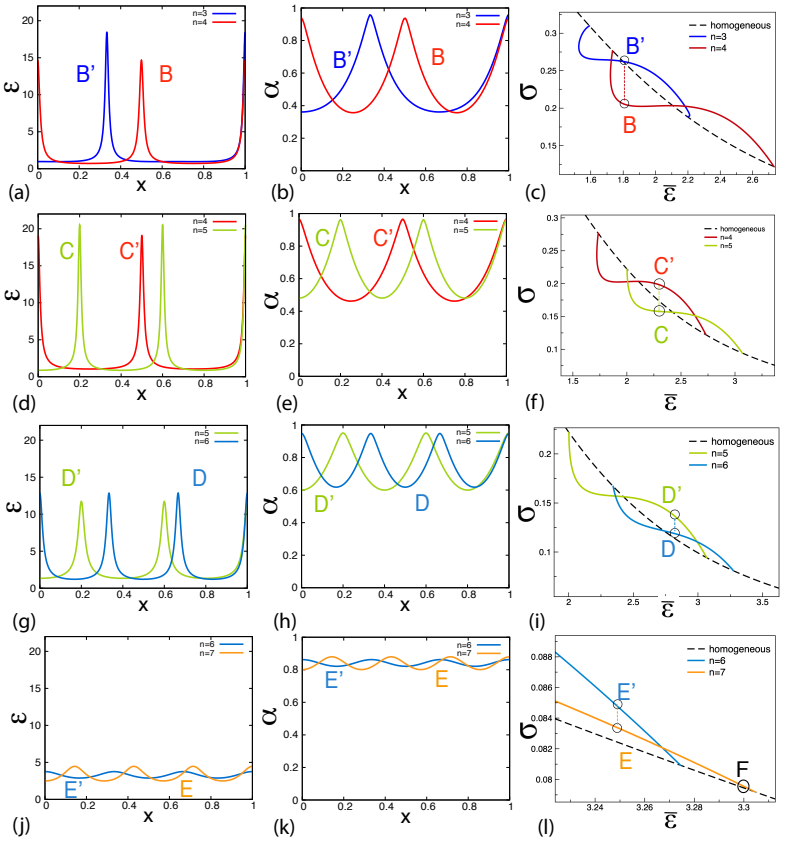

Figure 17: Phase-field modeling of a brittle bar on elastic foundation: strain (first column) and phase-field (second column) profiles before and after various equilibrium (energy minimizing) transitions, see Figs. 16(a,b). The third column shows the stress-jump at the crossing points. Parameters: $\lambda_1 = 0.158$, $\lambda_2 = 0.34$.

The non-affine branches in Fig. 16 describe the successive failure patterns developing in the process of quasi-static stretching. The nature of these patterns is illustrated in Fig. 17 where, for the sake of easier comparison with Fig. 11, we show again the succession of transitions along the global minimum path.

The transition B'→B shows how the non-symmetric, two-crack configuration, which is a deformed version of the first non-affine configuration A nucleated at G, transforms into the symmetric three-crack configuration with one

localized crack in the center and two localized cracks close to the boundaries. Then, the transition C'→C breaks the symmetry again creating a three-crack configuration with two localized cracks inside and one localized crack on the boundary. The symmetry is again recovered during the transition D'→D when the four-crack configuration emerges with two localized cracks inside and two localized cracks on the boundaries. Finally, after yet another symmetry breaking transition E'→E the affine configuration is recovered at F.

Our analysis shows that in the phase-field model of a stretched brittle bar, cracks remain localized even in the presence of an elastic background. Their number increases with stretch till the state is reached when localized cracks disappear because the system response becomes entirely dominated by the elastic background. Despite the presence of such a background, the extended damage zones containing distributed micro-cracks do not appear, and, instead, failure takes the form of a pattern built of smeared out but sharply isolated displacement discontinuities. In this sense, the reinforcement through an elastic embedding is not equivalent to the reinforcement brought about by floppy bending dominated sub-structure. Such sub-structure is, therefore, a crucial element of the proposed failure de-localization design.

6. Conclusions

While some natural materials break with the formation of a single macro-crack, others exhibit diffuse macro-cracking. The difference is reflected in the nomenclature of fracture and damage mechanics. Since both of these failure modes may become relevant in the same applications, it is of interest to design artificially engineered materials that can switch from one mode to another.

With this aim in view, we proposed in this paper a conceptual design of a high-toughness, pseudo-ductile meta-material with nominally brittle sub-elements. The idea is to transform a brittle structure, which normally fails with the formation of highly localized cracks, into an apparently ductile structure exhibiting de-localized damage. The desired nominal ductility is achieved by coupling a conventional brittle sub-structure with a reinforcing floppy sub-structure that can transmit bending-dominated nonlocal elastic interactions. It is now feasible to 3D print the implied high-contrast composite networks with inextensible but bendable elements.

To demonstrate the main effect, we solved a series of rather elementary model problems showing how the presence of a floppy sub-structure can suppress strain localization and induce the formation of diffuse zones of micro-cracking. The analysis is based on the asymptotically equivalent continuum theory of GL type with strain as the order parameter. Since the local part of the corresponding GL energy is represented by a single-well potential with sub-linear growth, the nonlocal (gradient) term becomes relevant 'volumetrically' even though there is a small coefficient in front of it. This is unusual given that in the conventional theory of phase transitions, similar term is only important in narrow transition zones. In tensile loading, the proposed GL model reproduces adequately the behavior of the original discrete model, including the intriguing re-entrant bifurcation. The presence in the space of the loading parameters of a finite range where the mechanical response of the system is non-affine may be of interest to applications. It implies that under monotone driving, the appropriately designed meta-material can produce a transient, information-carrying failure pattern that first comes out but then gets erased.

The discussed prototypical design of the pantograph-reinforced mass-spring chain serves only as a proof of concept. The industrially relevant 3D brittle meta-materials, reinforced by bending dominated floppy networks, would still have to be designed. Future work in this direction must also include the account of irreversibility of damage and the development of rigorous finite strain continuum approximation accounting for both 'local' and 'nolocal' sub-structures.

7. Acknowledgments

The authors are grateful to G. Vitale for his various contributions to the initial version of this paper. O.U.S. was supported by the grant ANR-19-CE08-0010-01 and L.T. by the grant ANR-10-IDEX-0001-02 PSL.

References

[1] Bertram Broberg K. Cracks and Fracture. Elsevier; 1999.
[2] by Hans J. Herrmann E, Roux S. Statistical Models for the Fracture of Disordered Media. Elsevier; 1990.
[3] Kanninen MF, Popelar CL. Advanced fracture mechanics. Oxford University Press; 1985.
[4] Truskinovsky L. Fracture as a phase transition. Contemporary research in the mechanics and mathematics of materials 1996;322-332.
[5] Triantafyllidis N, Aifantis E. A gradient approach to localization of deformation. i. hyperelastic materials. Journal of Elasticity 1986;16(3):225–37.

[6] Belytschko T, Chen H, Xu J, Zi G. Dynamic crack propagation based on loss of hyperbolicity and a new discontinuous enrichment. Int J Numer Meth Engng 2003;58(12):1873–905.

[7] Baker I, Munroe PR. Improving intermetallic ductility and toughness. Journal of Metals 1988;40(2):28–31.

[8] Swadener JG, Baskes MI, Nastasi M. Molecular dynamics simulation of brittle fracture in silicon. Phys Rev Lett 2002;89(8):085503.

[9] Evans AG, Faber KT. Toughening of ceramics by circumferential microcracking. J Am Ceram Soc 1981;64(7):394–8.

[10] Faber KT, Iwagoshi T, Ghosh A. Toughening by stress-induced microcracking in two-phase ceramics. J Am Ceram Soc 1988;71(9):C–399.

[11] Driscoll MM, Chen BGg, Beuman TH, Ulrich S, Nagel SR, Vitelli V. The role of rigidity in controlling material failure. Proceedings of the National Academy of Sciences 2016;113(39):10813–7.

[12] Budiansky B, Hutchinson JW, Lambropoulos JC. Continuum theory of dilatant transformation toughening in ceramics. Int J Solids Struct 1983;19(4):337–55.

[13] Green DJ. Transformation Toughening Of Ceramics. 1st edition ed.; CRC Press; 2018.

[14] Del Piero G, Truskinovsky L. Macro- and micro-cracking in one-dimensional elasticity. Int J Solids Struct 2001;38(6):1135–48.

[15] Cherkaev A, Slepyan L. Waiting element structures and stability under extension. Int J Damage Mech 1995;4(1):58–82.

[16] Wiederhorn SM. Brittle fracture and toughening mechanisms in ceramics. Annu Rev Mater Sci 1984;14(1):373–403.

[17] Davies TJ, Ogwu AA. A possible route to improving the ductility of brittle intermetallic compounds. J Alloys Compd 1995;228(1):105–11.

[18] Yang T, Zhao YL, Liu WH, Zhu JH, Kai JJ, Liu CT. Ductilizing brittle high-entropy alloys via tailoring valence electron concentrations of precipitates by controlled elemental partitioning. Materials Research Letters 2018;6(10):600–6.

[19] Borja da Rocha H, Truskinovsky L. Rigidity-Controlled crossover: From spinodal to critical failure. Phys Rev Lett 2020;124(1):015501.

[20] Daniel R, Meindlhumer M, Baumegger W, Zalesak J, Sartory B, Burghammer M, et al. Grain boundary design of thin films: Using tilted brittle interfaces for multiple crack deflection toughening. Acta Mater 2017;122:130–7.

[21] Ebrahimi MT, Balint DS, Sutton AP, Dini D. A discrete crack dynamics model of toughening in brittle polycrystalline material by crack deflection. Eng Fract Mech 2019;214:95–111.

[22] Wu H, Fan G. An overview of tailoring strain delocalization for strength-ductility synergy. Prog Mater Sci 2020;113:100675.

[23] Liang F, Zhang B, Yong Y, Luo XM, Zhang GP. Enhanced strain delocalization through formation of dispersive micro shear bands in laminated ni. Int J Plast 2020;132:102745.

[24] Radi K, Jauffres D, Deville S, Martin CL. Strength and toughness trade-off optimization of nacre-like ceramic composites. Composites Part B 2020;183:107699.

[25] Buxton GA, Clarke N. "bending to stretching" transition in disordered networks. Phys Rev Lett 2007;98(23)(238103).

[26] Broedersz CP, MacKintosh FC. Modeling semiflexible polymer networks. Rev Mod Phys 2014;86:995–1036.

[27] Zadpoor AA. Mechanical meta-materials. Materials Horizons 2016;3(5):371–81.

[28] Alibert JJ, Seppecher P, Dell'Isola F. Truss Modular Beams with Deformation Energy Depending on Higher Displacement Gradients. Mathematics and Mechanics of Solids 2003;8:51–73.

[29] van der Giessen E. Materials physics: Bending maxwell's rule. Nat Phys 2011;7(12):923–4.

[30] Maxwell JC. L. on the calculation of the equilibrium and stiffness of frames. The London, Edinburgh, and Dublin Philosophical Magazine and Journal of Science 1864;27(182):294–9.

[31] Calladine CR. Buckminster fuller's "tensegrity" structures and clerk maxwell's rules for the construction of stiff frames. Int J Solids Struct 1978;14(2):161–72.

[32] Schenk M, Guest SD. On zero stiffness. Proc Inst Mech Eng Part C 2014;228(10):1701–14.

[33] Pideri C, Seppecher P. A second gradient material resulting from the homogenization of an heterogeneous linear elastic medium. Continuum Mechanics and Thermodynamics 1997;9(5).

[34] Cherednichenko KD, Smyshlyaev VP, Zhikov VV. Non-local homogenized limits for composite media with highly anisotropic periodic fibres. Proceedings of the Royal Society of Edinburgh: Section A Mathematics 2006;136(01).

[35] Camar-Eddine M, Seppecher P. Determination of the closure of the set of elasticity functionals. Arch Ration Mech Anal 2003;170(3):211–45.

[36] Boutin C, Soubestre J, Dietz MS, Taylor C. Experimental evidence of the high-gradient behaviour of fiber reinforced materials. European Journal of Mechanics-A/Solids 2013;42.

[37] Bacca M, Bigoni D, Dal Corso F, Veber D. Mindlin second-gradient elastic properties from dilute two-phase cauchy-elastic composites. part i: Closed form expression for the effective higher-order constitutive tensor. Int J Solids Struct 2013;50(24):4010–9.

[38] Truskinovsky L, Zanzotto G. Ericksen's bar revisited : Energy wiggles. J Mech Phys Solids 1996;44(8):1371–408.

[39] Golubović L, Lubensky TC. Nonlinear elasticity of amorphous solids. Phys Rev Lett 1989;63(10)(1082).

[40] Marconi VI, Jagla EA. Diffuse interface approach to brittle fracture. Phys Rev E 2005;71:036110.

[41] Triantafyllidis N, Bardenhagen S. On higher order gradient continuum theories in 1-d nonlinear elasticity. derivation from and comparison to the corresponding discrete models. Journal of Elasticity 1993;33(3):259–93.

[42] Placidi L. A variational approach for a nonlinear 1-dimensional second gradient continuum damage model. Continuum Mech Thermodyn 2015;27:623–38.

[43] Le DT, Marigo JJ, Maurini C, Vidoli S. Strain-gradient vs damage-gradient regularizations of softening damage models. Comput Methods Appl Mech Eng 2018;340:424–50.

[44] Fokoua L, Conti S, Ortiz M. Optimal scaling in solids undergoing ductile fracture by void sheet formation. Arch Ration Mech Anal 2014;212(1):331–57.

[45] Fokoua L, Conti S, Ortiz M. Optimal scaling laws for ductile fracture derived from strain-gradient microplasticity. J Mech Phys Solids 2014;62:295–311.

[46] Zhang L, Lake SP, Barocas VH, Shephard MS, Picu RC. Cross-linked fiber network embedded in an elastic matrix. Soft Matter 2013;9:6398–405.

[47] Frémond M, Nedjar B. Damage, gradient of damage and principle of virtual power. Int J Solids Struct 1996;33(8):1083–103.

[48] Bourdin B, Francfort GA, Marigo JJ. Numerical experiments in revisited brittle fracture. J Mech Phys Solids 2000;48(4):797–826.
[49] Lorentz E, Andrieux S. Analysis of non-local models through energetic formulations. Int J Solids Struct 2003;40(12):2905–36.
[50] Benallal A, Marigo JJ. Bifurcation and stability issues in gradient theories with softening. Modell Simul Mater Sci Eng 2006;15(1):S283.
[51] Ambrosio L, Tortorelli VM. Approximation of functional depending on jumps by elliptic functional via t-convergence. Communications on Pure and Applied Mathematics 1990;43(8):999–1036.
[52] Aranson IS, Kalatsky VA, Vinokur VM. Continuum field description of crack propagation. Phys Rev Lett 2000;85(1):118–21.
[53] Karma A, Kessler DA, Levine H. Phase-field model of mode iii dynamic fracture. Phys Rev Lett 2001;87:045501.
[54] Eastgate LO, Sethna JP, Rauscher M, Cretegny T, others . Fracture in mode I using a conserved phase-field model. Physical review E 2002;.
[55] Puglisi G, Truskinovsky L. Thermodynamics of rate-independent plasticity. J Mech Phys Solids 2005;53(3):655–79.
[56] Bochkanov S, Bystritsky V. Alglib. Available from: www alglib net 2013;.
[57] Chan TFC, Keller HB. Arc-Length continuation and multigrid techniques for nonlinear elliptic eigenvalue problems. SIAM J Sci and Stat Comput 1982;3(2):173–94.
[58] Alibert JJ, Seppecher P, Dell'Isola F. Truss modular beams with deformation energy depending on higher displacement gradients. Math Mech Solids 2003;8(1):51–73.
[59] Charlotte M, Truskinovsky L. Linear elastic chain with a hyper-pre-stress. J Mech Phys Solids 2002;50(2):217–51.
[60] Braides A, Truskinovsky L. Asymptotic expansions by Γ-convergence. Continuum Mech Thermodyn 2008;20(1):21–62.
[61] Truskinovsky L, Vainchtein A. The origin of nucleation peak in transformational plasticity. J Mech Phys Solids 2004;52(6):1421–46.
[62] Dellwo D, Keller HB, Matkowsky BJ, Reiss EL. On the birth of isolas. SIAM Journal on Applied Mathematics 1982;42(5).
[63] Vainchtein A, Healey TJ, Rosakis P. Bifurcation and metastability in a new one-dimensional model for martensitic phase transitions. Computer Methods in Applied Mechanics and Engineering 1999;170(3–4):407 –21.
[64] Ren X, Truskinovsky L. Finite scale microstructures in nonlocal elasticity. Journal of Elasticity 2000;59(1-3):319–55.
[65] Doedel EJ, Champneys AR, Dercole F, Fairgrieve T, Kuznetsov Y, Oldeman B, et al. AUTO-07P: Continuation and Bifurcation Software for Ordinary Differential Equations; 2008. URL: http://sourceforge.net/projects/auto-07p/.
[66] Pham K, Marigo JJ, Maurini C. The issues of the uniqueness and the stability of the homogeneous response in uniaxial tests with gradient damage models. J Mech Phys Solids 2011;59(6):1163 –90.
[67] Mindlin R. Micro-structure in linear elasticity. Arch Ration Mech Anal 1964;16:51–78.